Journal of NAMP 67, 2 (2024) 145-158

The Nigerian Association of Mathematical Physics

Journal homepage: https://nampjournals.org.ng

Study of the structure and defect chemistry of ThO_2 as a nuclear fuel.

Edwin Humphrey Uguru[1,2]

[1] *Department of Industrial Physics, David Umahi Federal University of Health Sciences, P.M.B 211, Uburu, Nigeria*

[2]*International Institute for Nuclear Medicine and Allied Health Research, David Umahi Federal University of Health Sciences, PMB 211, Uburu, Ebonyi State, Nigeria*

ARTICLE INFO

Article history:
Received xxxxx
Revised xxxxx
Accepted xxxxx
Available online xxxxx

Keywords:
Thorium dioxide,
GULP,
Potential models,
Atomistic simulation,
Defect.

ABSTRACT

Thorium fuel cycle is a globally known nuclear fuel alternative, having good physical, neutronic, and chemical properties. However, there are limited knowledge on the potentials, models, and mechanical properties of ThO_2 compared to UO_2. Thus, the present study investigated the structural properties and defect chemistry of ThO_2 by atomistic computer simulation technique using General Utility Lattice Programme (GULP) code. The structural properties were calculated which showed good agreement with the literature. The defects formation energies in ThO_2 of the isolated and cluster atoms are calculated. It is found that the interstitial Th^{4+} defect is the most probable defect with an energy release of 60.19 eV, while oxygen Frenkel pair is the most energetically probable for defect cluster. The good agreement shown between the present simulation results with the experimental values supports the validity of the method and the structural and mechanical suitability of ThO_2 as a potential nuclear fuel.

1. Introduction

Thorium-based nuclear fuel is considered a potential material for future use in many reactor types [1]. Interests in thorium-based fuel cycle are based on the concerns generated by the continuous use of uranium dioxide fuel cycle in reactor operations [2]**.** These concerns include the vast production of plutonium, sustainability of uranium, production of transuranic isotopes and long-lived actinides, radiotoxicity of nuclear waste, proliferation, and nuclear terrorism [3]. Indeed, thorium fuel cycle offers the potential for more abundant nuclear material and safer nuclear fuel alternative to uranium fuel cycle [3, 4). Under irradiation, thorium fuel has shown good structural (both physical and thermochemical) stability, reliable neutronic properties, higher burn-up, and generates less actinide wastes compared to uranium and plutonium fuel cycles [5].

*Corresponding author: Edwin Humphrey Uguru
E-mail address: : uguruedddy2008@yahoo.com
https://doi.org/10.60787/jnamp.v67i2 .363
1118-4388© 2024 JNAMP. All rights reserved

Thorium is a fertile nuclear material, with six (6) of its naturally occurring isotopes in trace amount while ^{232}Th has the largest abundance of 99.98%, having half-life, $T_{1/2} = 1.405 \times 10^{10}$ years. In a nuclear reactor, ^{232}Th undergoes nuclear transmutation by thermal neutron absorption reaction and beta decays to produce a fissile ^{233}U nuclide. In an oxide form, ThO_2 has a more stable structural, thermophysical and thermodynamic properties compared to UO_2 and PuO_2, and it is also distinguished over uranium and plutonium oxides due to its single oxidation state of (+4) [6] unlike UO_2 fuel that has oxidation state from 2 to 6 with a complex range of stoichiometry in U-O system [7]. This single oxidation state of +4 in compounds makes it less reactive with minerals. The implication is that thorium dioxide has a low number of oxygen vacancies and interstitial defects, showing a very little non-stoichiometry. These properties are reflected on the high thermal conductivity, high thermal stability (high melting temperature), low chemical reactivity, lower thermal expansion coefficient of thorium dioxide compared to uranium and plutonium dioxides [8].

In the literature, information on the potential, models, structural, and defect chemistry of ThO_2 are not as comprehensive as UO_2. Moreover, there is not much atomistic simulation studies in the literature for pure ThO_2 unlike UO_2 apart from the notable experimental results for pure ThO_2 by Lang *et al.* [9] and Macedo *et al*. [10], while Osaka *et al.* [11] reported the atomistic simulation of Gadolinium-doped ThO_2 using MXDORTO molecular dynamics simulation code.

The reliability of any simulation is greatly determined by the interatomic potentials of the system and the number of ionic clusters defined by the applied periodic boundary conditions. In the derivation of these potentials, both non-empirical and empirical potentials methods have been successfully used, but the empirical potentials procedures prove to be more efficient due to an extra component of flexibility and reliability incorporated over non-empirical potentials [12]. The empirical potential though not as accurate as the first principle of calculations, can simulate close to billions of atoms at non-zero temperature [13]. Thus, they were widely used to calculate the elastic and bulk properties, defects, and other dynamic properties of UO_2 nuclear fuel. From the available literature as reported by Behera and Deo [13]. The literature showed that Osaka *et al.* [11] and Nadeem *et al.* [12] provided the empirical potential for ThO_2, which was adopted in this study.

In this work, use was made of the potentials and models satisfactorily used for the atomistic simulation of UO_2 to determine their efficiency and reproducibility on the potentials and models of ThO_2. Atomistic simulation of ionic oxides is a popular research methodology and has been found successful in calculating the structural, interatomic potentials, bulk properties, defects etc. of ionic compounds such as uranium and thorium oxides [12, 13].

The atomistic simulation was performed using BlueBEAR HPC network service, at the University of Birmingham, England, United Kingdom, adopting defined interatomic potential models [12, 14] and General Utility Lattice Programme (GULP) simulation code [15]. The oxygen-oxygen (O-O) empirical potential interactions like tetravalent UO_2 full rigid-ionic models are adopted for ThO_2 investigation [13]. The UO_2 potentials have the same O-O interaction with same charges, hence, ThO_2 based on this O-O interaction will be same as that of UO_2.

The thorium-thorium (Th-Th) and thorium-oxygen (Th-O) interactions were investigated by fitting the lattice parameters, elastic, and static dielectric constant [12]. The atomistic computer simulation specifies the interatomic potential models which predict the properties of the simulated system by describing the energy variation of the cluster atoms as a function of their co-ordinates [13], and these models, therefore, determine the viability of the atomistic computer simulation studies [12].

2. Computational methodology

The General Utility Lattice Program (GULP) is a code for performing high power computer (HPC) simulations on complex solids and clusters [16]. This code is embedded simulation algorithms for 3-D periodic systems. It is found to exhibits an increased computational efficiency and takes care of symmetric, inorganic, and organic systems unlike the standard algorithm which does not account for symmetry. The method used in this work is the same as that used for UO_2 [14], and all the calculations made are contained within GULP code [16]. The computational simulation flow chart is shown in figure 1. However, some salient features of ThO_2 relevant to the present simulation are discussed below and the computational theories presented in subsequent subsections.

To obtain the most suitable configuration of the crystal structure of the ThO_2; structural optimization of parameters such as lattice parameter, kinetic energy cutoff and k-point by relaxing its structure and minimizing its total energy. Additionally, it involves using optimized lattice parameter to calculate its properties, converging the kinetic energy cutoff and k-point grid for accurate results.

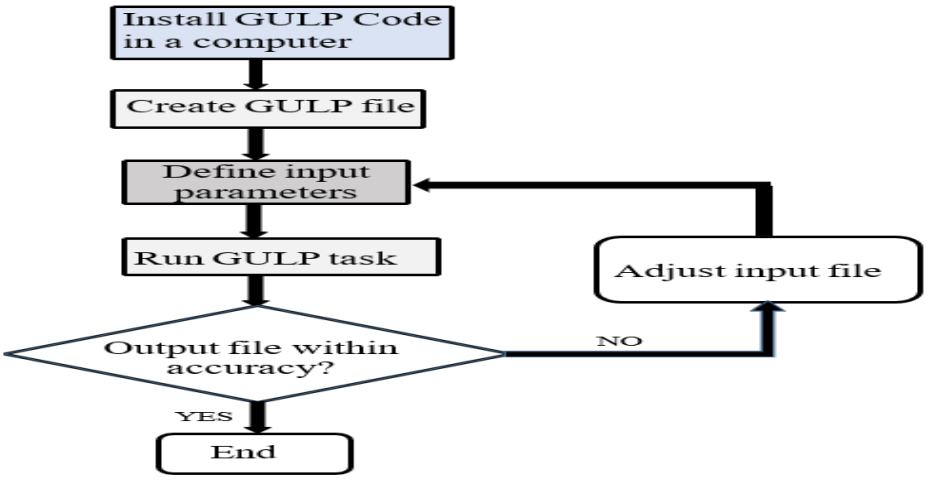

Figure 1: A flow chart of the simulation process.

ThO_2 has face centred cubic lattice crystal structure like UO_2 and PuO_2, and it can be heated to melt without phase transition, thereby showing great structural similarities. For ThO_2 that has a cubic fluorite structure with $Fm\bar{3}m$ symmetry and #225 space group, the ions are arranged in such a way that thorium (Th) ions occupy the face centred position while oxygen (O) ions occupy the tetrahedral positions. Thorium dioxide has majorly ionic bond in its lattice structure. The basic forces that exist in the system are coulombic (long-range potential) and non-coulombic (short-range potential) forces. Therefore, the pair interactions (Th-Th, Th-O, and O-O) within the ThO_2 required to simulate the system are long-range and short-range interactions [6, 17]. Consequently, adding together the short-range forces can easily converge the interactions in real space till the associated terms become accurately negligible. But other terms decay slowly as a function of distance, mostly because the number of interactions increases as $4\pi r^2 N_p$, where r, is the separation distance, and N_p is the particle number density. For long-range forces, the system is conditionally convergent as it follows inverse square law ($\frac{1}{r^2}$) [16]. This indeed, justifies the need to consider the two classes of energy components separately.

The charge system of ThO_2 shows a formal charge model of 4+ and 2- for Th and O respectively, and a partial charge model for any other type of charge description on Th and O ions. To incorporate the effect of polarization of the ions, a shell model description is included in the system. In effect, each ion is described by a core and shell of the model whose sum is the ionic

charge. The values of the core and shell of ThO_2 in GULP input file were chosen to accommodate temperature dependence of the lattice parameter. The core and shell are connected either by harmonic or anharmonic spring oscillator. The coupled potential for harmonic spring is given by equation 1.

$$V(\omega) = ½k_2\omega^2 \quad (1)$$

where ω is the core-shell displacement and k_2 is the harmonic spring constant.

2.1 Long-range potential interactions

For inorganic materials, the coulomb term of the potential is the dominant term for the calculation of its interatomic potentials, especially for oxides [16]. However, the long-range interactions in a system are described by the coulomb interaction term as in equation (2).

$$V_{coul}(r_{ij}) = \frac{1}{2}\sum_{i=1}^{N}\left\{\sum_{j\neq i}\frac{q_i q_j}{r_{ij}}\right\} \quad (2)$$

where, N is the total number of ions in the system, while q_i and q_j are the magnitude of charges on the ions i and j, and r_{ij} is the separation between ions i and j. Consequently, for small and moderate size systems, the Ewald summation approach is efficiently employed to calculate the coulomb interactions within a finite cut-off distance [13].

2.2 Short-range potential interactions

The short-range forces act on the shell while the long-range force act on both core and shell of the atom. The short-range interactions are in principle more difficult to describe because they involve many components. These interactions include that of electron cloud overlap, van der Waal and Pauli repulsion. It is worthy to say that the short-range interaction considers electron polarizability [14].

Indeed, the dominant short-range potential description used is the "Buckingham potential" shown in equation (3), which consists of a repulsive exponential and an attractive dispersion term between pairs of species.

$$V_{Buck}(r_{ij}) = A_{ij}exp\left(-r_{ij}/\rho_{ij}\right) - C_{ij}/r_{ij}^6 - D_{ij}/r_{ij}^8 \quad (3)$$

where A, ρ, C and D are constants that can be derived by empirical fitting. The free parameters A and ρ are measures of the size and hardness of the ions of the system while C_{ij}/r_{ij}^6 term describes attraction within the system due to dispersive, covalent, and Van der Waals forces [12]. Generally, these constants represent the pair-wise repulsion coefficient between electron clouds, radii of the ions of the atoms, and the coefficient of the dispersion term which are due to the existing dipoles between the core and the electrons of the interacting atoms.

There exist a few other short-range potentials aside Buckingham potential, which can be used for ionic oxides. An example is the Buckinham-4 potential which tries to ignore the unphysical attractive forces between the ions at very short distances which is given in equation (4) [13]. The short-range input parameters for anion-anion and cation-anion lattice potential interactions are presented in Table 1 and 2 respectively.

$$\begin{array}{ll} V_{Buck\,4}(r_{ij}) = A_{ij}\exp\left(-r_{ij}/\rho_{ij}\right) & if\ r_{ij} \leq r_1 \\ 5th\ order\ polynomial & if\ r_1 < r_{ij} \leq r_{min} \\ 3rd\ order\ polynomial & if\ r_{min} < r_{ij} \leq r_2 \end{array} \quad (4)$$

$C_{ij}/r_{ij}^6 \quad if\ r_{ij} > r_2$

where, r_{ij} is the separation between two ions i and j, and A, ρ, C, r_1, r_{min}, and r_2 are constants. Another example is the Morse potential [7] represented in equation (5), which is specifically used in describing the interactions in covalent bonded materials.

$$V_{morse}(r_{ij}) = D_{ij}\{[1 - \exp(-\beta_{ij}(r_{ij} - r_{ij^*}))]^2 - 1\} \quad (5)$$

Where r_{ij} is the separation between the two ions i and j, while D, β and r_{ij^*} are constants.

Table 1

The anion-anion lattice potential for O^{2-} –O^{2-} interaction [11].

Potential interaction	Short-range parameters			Shell model[a]	
	A (eV)	ρ (Å)	C (eV Å^6)	Y IeI	K_2(eV Å^{-2})
O^{2-} - O^{2-}	11272.6	0.1363	134.0	-4.4	296.2
	r_{min}	Cut_1	r_{min}	Cut_2	r_{max}
	0.0	1.2	2.1	2.6	15.0

[a] means that Y and k_2 are the shell charge and harmonic spring constant respectively.

Table 2

The cation-anion lattice potential for Th^{+4} –O^{2-} interaction.

Potential interaction	Short-range parameters		Shell model[b]	
	A (eV)	ρ (Å)	Y IeI	K_2 (eV Å^{-2})
Th^{+4} - O^{2-}	1147.7	0.3949	7.28	193.1

[b] means that Y and k_2 are the shell charge and spring constants for Th^{+4} respectively.

From Table 1, r_{max} is the short-range cut-off, and r_{min} defines the rest point of the function, which must be set minimum in the system, while cut_1 and cut_2 are the boundary points in which the first and second derivative of the function must be continuous.

2.3 Simulation techniques and energy minimisation

In atomistic computer simulation, two main methods are applied in the present computational technique. The first method is known as "force field". For good treatment/simulation of perfect and defect crystal lattices, the electronic structure of the system is summed into effective interatomic potentials (V). The interatomic potential describes in detail the variation in the energies of the substance or structure as a function of the nuclear co-ordinates (r_1……r_N) of the total number of atoms in the substance. Also, the total potential is generally partitioned into "pair", "three-body", "four-body", and other higher terms as seen in equation (6).

$$V(r_1..r_N) = \sum_{i,j=1}' v^{(2)}(r_{i,j}) + \sum_{i,j.k=1}' v^{(3)}(r_{i,}r_j,r_k) + \sum_{i,j,k,l=1}' v^{(4)}(r_i,r_j,r_k,r_l) + \quad (6)$$

The prime symbols on the summation sign indicate that a given term is only added once in the system. The total potential term V, is in most cases approximated to be equal to the pair potential term, which depends commonly on the separation between the nuclei, i and j.
For ionic systems/crystals whose interactions between the atoms are non-directional, this approximation is generally applied. But this is less acceptable for covalent bonded substances, which has strong directional interaction. Indeed, the pair potential term on its own is normally divided into coulomb and non-coulomb terms as in equation (7) [18, 19].

$$v^{(2)}(r_{ij}) = \frac{q_i q_j}{r_{ij}} + \phi(r_{ij}) \qquad (7)$$

where, q_i and q_j are the effective charges of the atoms, and r_{ij} is the separation between the ions i and j.
Furthermore, Buckingham and Lennard-Jones forms are some of the acceptable analytical functions used to describe the non-coulomb ϕ, part of the pair potential which are preferable for non-bonded interactions.

The major challenge in today's computational studies of molecules and solids is centred on how to attain high quality force field. To achieve this, the use of empirical fitting procedure is employed. Here, the parameters in the analytical function describing the potential are adequately adjusted through a least-squares fitting method. By doing so, it reproduces accurately the observed properties of the crystal.
The second is the "quantum mechanical" method, which has been used in the past years to calculate the potentials of crystals.
Therefore, the energy of a crystal, a pair or clusters of non-bonded atoms is calculated for different shapes and sizes. Finally, the change in the calculated energy is then fitted to an interatomic potential function [15].
To ensure efficient and optimised computational simulation, the input variables and energy minimisation processes were well defined. The many energy minimisation processes embedded in GULP code is carefully used to achieve optimisation. The system can be optimised at constant pressure where all the cell variables are considered or at volume in which the unit cell remains frozen. However, other energy minimisation processes embedded in GULP that are of importance are; the Newton-Raphson, Broyden-Fletcher-Goldfarb-Shanno (BFGS) algorithm, and Rational Function Optimizer (RFO) which remove imaginary modes from hessian matrix in Newton-Raphson, thereby making the convergence of the system to be achieved quickly [16]. Equation (8) shows the relationship between energy minimisation search directions X, the hessian matrix H, and g, is the corresponding gradient vector.

$$X = H^{-1}g \qquad (8)$$

2.4 Defect energy

In view of the impact of defects on the viability of nuclear fuel under irradiation, the structural stability of ThO_2 is investigated by systematically calculating the formation energy of different kinds of defects. To calculate the formation energies, the positions of all ions are fully relaxed before the electronic free energies of the system with different defects are calculated.
However, the popular Mott-Littleton approach [20] is adopted in calculating the defect energies of the system. In doing this, the crystal structure with the defect is partitioned into three regions namely, regions I and IIa as shown in figure 2, and the unlabelled region IIb. The volume of the crystal that contains the defects is region I, and region IIa is the bulk crystal while region IIb represents the transition between regions I and IIa. In the process, region I is allowed to relax fully,

while some element of relaxation is allowed for region IIb only [13]. The radii which determine the region size used in this study is 14Å and 28Å for region I and IIa respectively like those used for UO_2 [14].

The lattice of ions surrounding the defect can relax in the total energy minimisation procedure using the previously described Mott-Littleton approach. The individual point defect (vacancy and interstitial) energies are combined to predict Frenkel and Schottky defect formation energies.

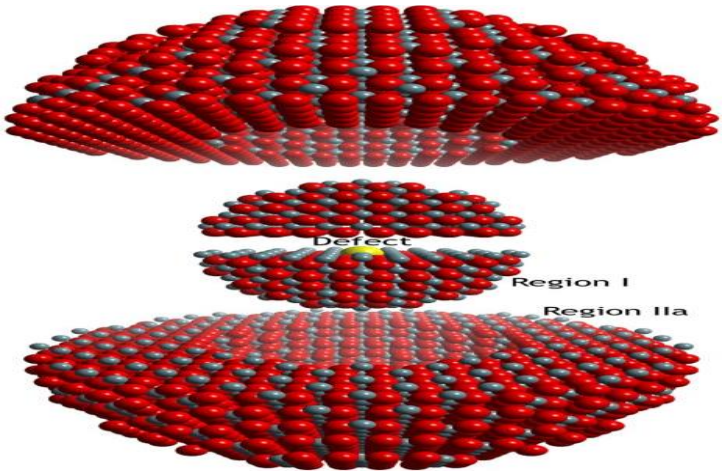

Figure 2: The Mott-Littleton structure of two region defect simulation [14].

3. Results and discussion

3.1. Structural and elastic properties

The observed structure of ThO_2 as shown in figures 3 (a) and (b) supports the fact that ThO_2 has a fluorite structure with $Fm\bar{3}m$ symmetry (#225 space group), showing face-centred cubic (fcc) lattice structure typical of ionic compounds like UO_2 and PuO_2 [21]. In the observed structure of ThO_2, Th ions (green coloured) occupy the face-centred position while O ions (red coloured) occupy tetrahedral sites at ± (¼, ¼, ¼) arrangement. In this study, Buckingham and Buckingham-Born-Mayer interatomic potential models are used to describe the ThO_2 interactions. Tables 1 and 2 provide the lattice potential for O^{2-}-O^{2-} (anion-anion) interactions achieved with Buckingham-4, and the lattice potential for Th^{4+}-O^{2-} (cation-anion) interaction using Buckingham-Born-Mayer, respectively.

These charged ions qTh = +4.0e- and qO = -2.0e are the formal charge models of the system without any partial charged model.

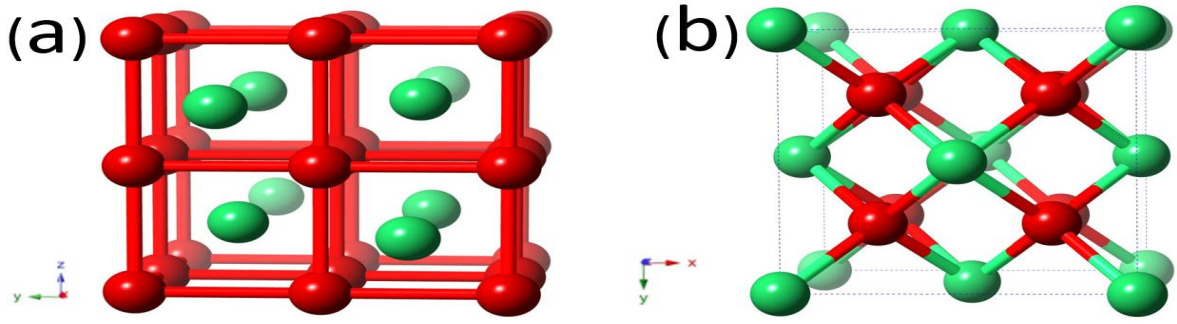

Figures 3 (a) and (b): The observed ThO_2 unit cells.

To estimate the lattice structure of ThO_2, each potential was geometrically optimized ensuring that the unit cell experiences total zero force in the system. For the calculation of elastic properties, the energy-volume relationship is employed with the applied strain in x, y, and z directions in the system. The bulk modulus was calculated by analysing the energy response of an equal strain applied in x, y, and z directions while the young modulus was calculated by considering the strain along one direction. The bulk modulus is a function of elastic constants, and therefore, was calculated using the zero-pressure adiabatic bulk modulus formula in equation (9). Table 3 shows the relationship between the calculated and experimental values of the potentials, and their percentage difference. Table 4 compared the properties of the calculated potentials of ThO_2 with available simulation results in the literature for ThO_2 and other ionic oxides, and different experimental methods such as full-potential linear muffin-tin orbital with generalised gradient approximation (FP-LMTO-GGA), X-ray diffraction (XRD), velocity of ultrasound and echo, and least-square fit used to achieve the results. The variation in the values of elastic constant especially in Table 4 affected the values of bulk modulus causing the larger difference compared to its similar values in Table 3.

$$B_o = \frac{1}{3}(C_{11} + 2C_{12}) \tag{9}$$

Table 3

The comparison of the calculated properties of ThO_2 with experimental values.

Potential properties	Calculated values	Experimental values	Oxides studied by experiment	Method used	Percentage difference (%)
Lattice parameter (Å)	5.6471	5.5997	ThO_2	Ultrasound	1.78
Volume ($Å^3$)	180.0832	175.59			2.56
Lattice energy (eV/ThO_2)	-99.7090	-104.64	Alkali Halide	Sound/echo	4.71
C_{11} (GPa)	436.42	367.0	ThO_2 at 25°C	Ultrasound	18.9
C_{12} (GPa)	85.15	106	ThO_2 at 25°C	Ultrasound	19.6
C_{44} (GPa)	32.51	79	ThO_2 at 25°C	Ultrasound	58.85
Bulk modulus (GPa)	202.24	198	UO_2 and ThO_2	X-ray diffraction	4.78
		198±2	ThO_2	FP-LTMO-GGA	3.71
Shear modulus (GPa)	48.23	95.6	Alkali Halide	Sound/echo	49.6
Young's modulus (GPa)	408.62	270	Alkali Halide	Sound/echo	51.34
Poisson's ratios	0.1633	0.279	ThO_2 at 25°C	Ultrasound	41.47
Compressibility (10^{-3} GPa^{-1})	4.94	4.16	Alkali Halide	Sound/echo	18.75
Static dielectric constant	29.67	18.9	UO_2 and ThO_2	Least-square fit	56.98
High frequency dielectric constant	3.53	4.86	UO_2 and ThO_2	Least-square fit	27.37

Table 4

Comparison of the calculated properties of ThO_2 with other calculated values for similar ionic oxides and doped ThO_2 from different authors in literature.

Potential properties	Calculated value	Ref [12]	Ref [11]	Ref [22]	Ref [19]	Ref [23]
Lattice parameter (Å)	5.6471	5.5946	5.5797	5.5995	5.6000	5.5998
Volume ($Å^3$)	180.08	175.11	173.71	175.61	175.61	175.60

Lattice energy (eV/ThO_2)	-99.7090	-104.970	-43.058	-101.348	-100.379	-100739
C_{11} (GPa)	436.42	573.0	441.0	367.0	367.0	366.0
C_{12} (GPa)	85.15	168.0	93.0	106.0	106.0	106.0
C_{44} (GPa)	32.51	132.0	86.0	105.0	103.0	97.0
Bulk modulus (GPa)	202.24	303.0	209.0	193.0	193.0	193.0
Shear modulus (GPa)	48.2	157.0	115.0	115.0	113.0	109.0
Young's modulus (GPa)	408.62	496.0	408.0	320.0	319.0	319.0
Poisson's ratios	0.1633	0.227	0.175	0.224	0.224	0.224
Compressibility (10^{-3} GPa^{-1})	4.94	3.30	4.78	5.19	5.19	5.19
Static dielectric constant	29.67	18.95	2.82	9.47	7.19	6.16
High frequency dielectric constant	3.53	4.42	-	-	-	-

In Table 4 for instance, Lewis and Catlow [22] studied ionic oxides, Nadeem et al [12] studied binary oxides, Walker et al. [19] and Osaka et al. [11] studied gadolinium-doped thorium dioxide. The calculated parameters are compared with the values obtained by these authors that studied oxides of fluorite structures using the same or different atomistic simulation techniques at different oxide conditions. This comparison is to determine the reproducibility of the developed potentials in fluorite structure of metal oxides. From Table 4, it is seen that the potentials regardless of simulation code and oxide type reproduced fairly the lattice parameter, which could be attributed to the non-transferability of shell parameters of oxides.

The good agreement of most of the parameters with the calculated values could be attributed to the reproducibility of these parameters for fluorite oxide structures since they have mostly ionic bonds. From Tables 5 and 6, the shear modulus for the calculated value is small compared to the other author's value. This may be due to the dependence of shear modulus on temperature and pressure for isotropic materials, since shear modulus decreases as temperature increases, and increases at high pressure unlike lattice parameter that decreases with pressure increase and increases with temperature [24, 25].

The Poisson's ratios for calculated and Osaka et al. [11] are closer but differed more with other author's values because they are of different metallic oxides. The difference between the results could be due to the presence of gadolinium in ThO_2. Table 4 shows that most of the parameters for the calculated and Osaka et al. [11] values agreed favourably except for lattice energy, shear modulus and static dielectric constant which is attributed to the presence of gadolinium in ThO_2 structure.

Furthermore, Table 6 shows that most of the parameters for Nadeem et al are higher than others because, it studied and simulated the molecular structure of the oxides instead of the atom. Generally, it is worthy to note that none of the experiments and simulations were conducted at same percentage concentration by weight and physical condition of the oxides, hence the noticed small and large variation in some of the parameters.

However, these values have proved the reliability, reproducibility, and functionality of interatomic potentials in computational simulation of ThO_2. The differences in some of the parameters could also be attributed to the variation made on the values of the charge for the core and shell model used in this study, and the limitations of the potential models for ThO_2. Hence, little adjustments are to be made on the potential models for high atomistic simulation efficiency of ThO_2 studies.

3.2. Thermal stability

Thermal stability of nuclear fuel under irradiation is critical for its application in nuclear industry, as the fuel would be subjected to a high temperature during operation. In view of this, the lattice parameter and specific heat capacity of ThO_2 were investigated as a function of temperature. The

computer simulation was done with a temperature range of 200 K – 1300 K. This indeed, shows the degree of thermal expansion of ThO_2, which agrees to a reasonable extent with experimental data.

Figures 4 and 5 present the variation of lattice parameter and heat capacity, respectively as the temperature increases from 200 K to 1300 K at constant pressure. The calculated thermal expansion of the lattice parameter in figure 4 shows that the lattice parameter of ThO_2 is 5.5Å, which agrees favourably with the lattice parameter of ≈ 5.6Å of the experimental value. The heat capacity at constant pressure shows a great stability as the temperature increases.

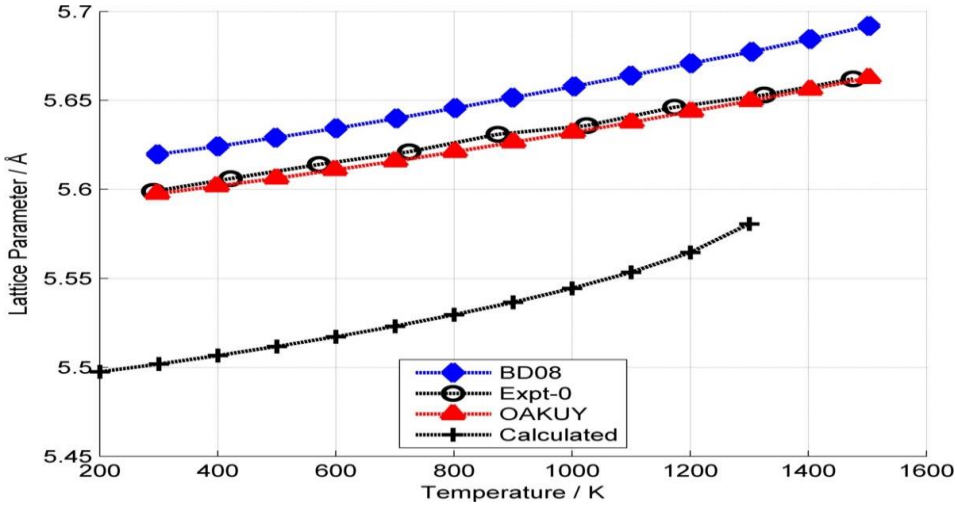

Figure 4: Variation of lattice parameter of ThO_2 with temperature and the correlation of BD08 [23], OAKUY [11], and Expt-o (experimental value).

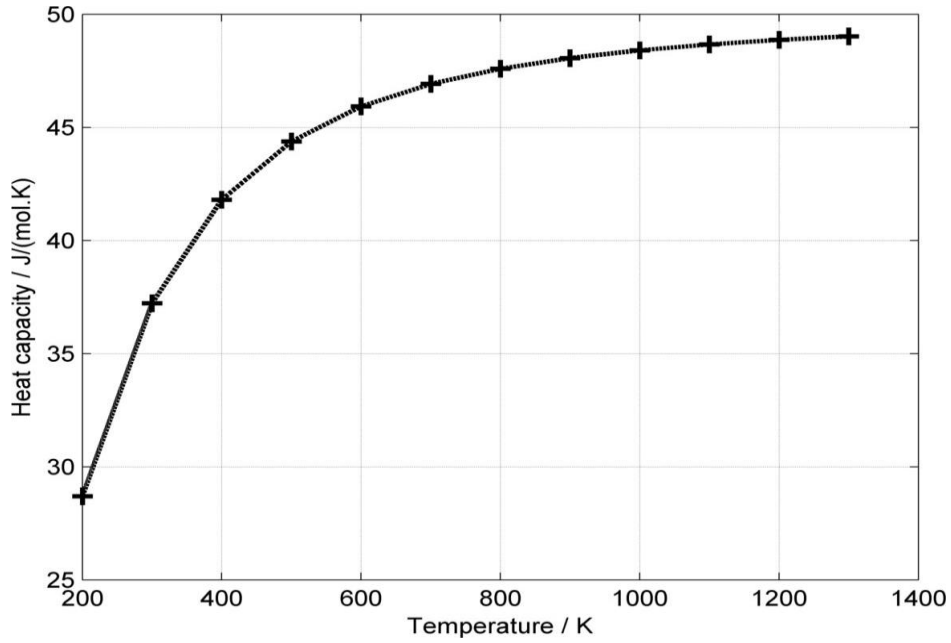

Figure 5: Variation of heat capacity with temperature at constant pressure.

Table 5 shows that the observed Th_i^{4+} and O_i^{2-} have negative formation energies. This depicts that the presence of Th_i^{4+} ions result in the formation of an interstitial Th_i^{4+} defect in ThO_2 with an energy release of 60.19 eV. Similarly, the interstitial of oxygen, O_i^{2-} is the most possible defect due to its small/negative formation energy. These two results reflect the ionic properties of Th-O bonds in that each thorium atom almost loses four electrons to two oxygen atoms in ThO_2. Also, the thorium vacancy has huge formation energy, and therefore, will be very difficult to form in intrinsic ThO_2.

Table 5
The calculated formation energies of an isolated atomic defect.

Type of defect	Position	Formation energy (eV)
Th^{+4} vacancy ($V_{Th}^{""}$)	(0, 0, 0)	78.92
O^{2-} vacancy ($V_O^{\cdot\cdot}$)	$\left(\frac{1}{4}, \frac{1}{4}, \frac{1}{4}\right)$	16.53
Th^{+4} interstitial $\left(Th_i^{\cdot\cdot\cdot\cdot}\right)$	$\left(\frac{1}{2}, \frac{1}{2}, \frac{1}{2}\right)$	-60.19
O^{2-} interstitial $\left(O_i''\right)$	$\left(\frac{1}{2}, \frac{1}{2}, \frac{1}{2}\right)$	-11.55

3.3. Cluster defect energy

Calculation of the formation energies in this manner assumes infinite dilution and omits the binding energy associated with the aggregation of point defects required to be considered to compare it with experimental observation. The results for the Frenkel pair clusters and ionic defect clusters are as presented in Tables 6 and 8 respectively, while Table 7 shows the formation energy of Th^{4+} and O^{2-} pair defect clusters.

3.3.1. Frenkel pair energy cluster

The Frenkel defects are represented by the reactions in equations (10) and (11) using Kröger-Vink Notation. The formation energies of oxygen and thorium Frenkel pairs at infinite distance are calculated while the defect clusters are simulated. The binding energy was calculated as the difference in the energy between the cluster and its constituent point defects (vacancies and interstitials) at infinite dilution.

For the simulations where the oxygen interstitial is placed near the vacancy, recombination is observed to occur during the geometry optimisation procedure unless the oxygen interstitial is constrained. To calculate the cluster energy, the oxygen defects were separated by a lattice of thorium ion as to help prevent recombination of the ions in the system. To achieve this, the two geometries for the oxygen Frenkel pair (OFP) were considered and the corresponding co-ordinates and resulting energies are presented in Table 8.

Frenkel Defects:

$$Th_{Th}^{\times} \rightleftharpoons V_{Th}'''' + Th_i^{\cdot\cdot\cdot\cdot} \quad (10)$$

$$O_O^{\times} \rightleftharpoons V_O^{\cdot\cdot} + O_i'' \quad (11)$$

Thorium Frenkel defect = 78.92 + (-60.19) = 18.73 (that is 9.37 eV per defect)

Oxygen Frenkel defect = 16.53 + (-11.55) = 4.98 (that is 2.49 eV per defect)

Table 6
Calculated formation energies of isolated atomic defect (Frenkel defects).

Type of defect	$V_O^{\cdot\cdot}$ position	O_i'' position	Formation energy (eV/defect)	Binding energy (eV/defect)
OFP 1	$\left(-\frac{1}{4},-\frac{1}{4},-\frac{1}{4}\right)$	$\left(\frac{1}{2},\frac{1}{2},\frac{1}{2}\right)$	1.77	-0.72
OFP 2	$\left(-\frac{1}{4},-\frac{1}{4},\frac{1}{4}\right)$	$\left(\frac{1}{2},\frac{1}{2},\frac{1}{2}\right)$	2.03	-0.46

3.3.2. Schottky defect energy cluster

The defect formation energies of the three types of vacancy cluster associated with the Schottky defects are shown in Table 7. The most energetically favourable position for the second oxygen vacancy is predicted to be in Schottky 1 configuration, and this was combined with the associated energy of forming ThO_2 at the surface to predict the Schottky defect energy. The summary of the Frenkel and Schottky defects of ThO_2 ionic cluster is presented in Table 8. The high value of Frenkel cation (thorium ion) defect energy supported the fact that it is difficult to create vacancies in the metal due to its large size [12].

Schottky defects:

The formation energy was calculated using the expression in equations (12), (13) and (14).

Defect energy =

$$Th_{Th}^{X} + 2O_O^{X} \leftrightharpoons V_{Th}^{''''} + 2V_O^{\cdot\cdot} + ThO_2\,(surf) \quad (12)$$

$$Th_{Th}^{X} \leftrightharpoons V_{Th}^{''''} + Th_i^{\cdot\cdot\cdot\cdot} \quad (13)$$

$$O_O^{X} \leftrightharpoons V_O^{\cdot\cdot} + O_i^{''} \quad (14)$$

$V_{Th}^{''''} + 2V_{O}^{\cdot\cdot} + ThO_{2\,(surf)}$ = 78.92 eV + (2 × 16.53) + (-102.12)

= 9.86 eV or 3.29 eV per defect (since there are three defects present).

Table 7
Calculated formation energies of Th^{4+} and O^{2-} pair defect clusters

Type of defect	Second $V_O^{\cdot\cdot}$ Position	Formation energy (eV/defect)	Binding energy (eV/defect)
Schottky 1	$\left(-\frac{1}{4},-\frac{1}{4},-\frac{1}{4}\right)$	35.90	-1.43
Schottky 2	$\left(-\frac{1}{4},\ \frac{1}{4},-\frac{1}{4}\right)$	35.94	-1.39
Schottky 3	$\left(-\frac{1}{4},\ \frac{1}{4},\ \frac{1}{4}\right)$	36.02	-1.32

Table 8
Calculated energies of ionic defect clusters

	Formation energy (eV/defect)	
Type of defect	Infinite dilution energy	Defect cluster energy
Thorium Frenkel pair	9.37	7.40
Oxygen Frenkel pair	2.49	1.77
Schottky defect	3.29	1.86

Conclusion

The method of atomistic computer simulation as an efficient technique in the derivation of interatomic potentials was used to investigate and determine the crystal structure and defect chemistry of ThO_2 as a potential nuclear fuel. This research work investigated the structural and defect chemistry of ThO_2, looking at its lattice parameter, Young's moduli, bulk modulus, shear, elastic constants, Schottky and Frenkel defects. The results justified the applicability of the potentials and models that was used in the literature for UO_2 fuel, which is used successfully on the computer simulation of ThO_2. It has also been demonstrated to be efficient in the calculation of intrinsic defects inherent in ThO_2 that contribute to the major solid-state properties of materials. The mechanical properties and crystallographic parameters of ThO_2 were calculated. The lattice expansion and heat capacity of ThO_2 were systematically investigated at different temperatures.

In addition to studying the mechanical properties of ThO_2, its structural stability was investigated by calculating the formation energy of different defects. The formation energies indicate that interstitial Th^{4+} is the most probable to appear in the ThO_2 with an energy release of 60.19eV. The Schottky defects and oxygen Frenkel pairs are seen to be the most energetically favourable form of intrinsic defect in ThO_2.

The results are found to be favourably in agreement with corresponding experimental measurements and other potentials models in the literature. The agreement between the calculated and experimental results proves the validity of the method and model used in this work. Therefore, the results support the suitability of ThO_2 as a nuclear fuel based on its structural and mechanical stability.

References

[1] Ault, T., Krahn, S., and Croff, A. (2017). Thorium fuel research and literature: Trends and insights from eight decades of diverse projects and elvolving priorities. *Annals of Nuclear Energy,* **110**, 726-738.

[2] Galahom, A. A. (2017). Minimization of the fission product waste by using thorium-based fuel instead of uranium dioxide. *Nuclear Engineering and Design,* **314**, 165-172.

[3] Schaffer, M. B. (2013). Abundant thorium as an alternative nuclear fuel: Important waste disposal and weapon proliferation advantages. *Energy Policy,* **60**, 4-12.

[4] Ünak, T. (2000). What is the potential use of thorium in the future energy production technology? *Progress in Nuclear Energy,* **37** (1), 137-144.

[5] Uguru, E. H., Abdul Sani, S. F., Khandaker, M. U., Rabir, M. H., Karim, J. A., Onah, D. U., and Bradley, D. A. (2021). Burn-up calculation of the neutronic and safety parameters of thorium-uranium mixed oxide fuel cycle in a Westinghouse small modular reactor. *International Journal of Energy Research*, **45**, 12013-12028.

[6] Lu, Y., Yang, Y., and Zhang, P. (2012). Thermodynamic properties and structural stability of thorium dioxide. *Journal of Physics: Condensed Matter,* **24**, 225801.

[7] Williams, N. R., Molinari, M., Parker, S. C., & Storr, M. T. (2015). Atomistic investigation of the structure and transport properties of tilt grain boundaries of UO_2. *Journal of Nuclear Materials,* **458**, 45-55.

[8] Chang, H., Yang, Y., Jing, X., and Xu, Y. (2006). Thorium-based fuel cycles in the modular high temperature reactor. *Tsinghua Science and Technology,* **11**, 731-738.

[9] Lang, S., and Knudsen, F. (1956). Some physical properties of high-density thorium dioxide. *Journal of the American Ceramic Society*, **39**, 415-424.

[10] Macedo, P., Capps, W., and Wachtman, J. (1964). Elastic constants of single crystal ThO2 at 25° C. *Journal of the American Ceramic Society*, **47**, 651-651.

[11] Osaka, M., Adachi, J., Kurosaki, K., Uno, M., and Yamanaka, S. (2007). Molecular dynamics study on defect structure of gadolinia-doped thoria. *Journal of Nuclear Science and Technology,* **44**, 1543-1549.

[12] Nadeem, M., Akhtar, M., Shaheen, R., Haque, M., and Khan, A. (2001). Interatomic potentials for some binary oxides. *Journal of Materials Science and Technology,* **17**, 638-642.

[13] Behera, R. K., and Deo, C. S. (2012). Atomistic models to investigate thorium dioxide (ThO_2). *Journal of Physics: Condensed Matter,* **24**, 215405.

[14] Read, M. S., and Jackson, R. A. (2010). Derivation of enhanced potentials for uranium dioxide and the calculation of lattice and intrinsic defect properties. *Journal of Nuclear Materials,* **406**, 293-303.

[15] Bird, R. A., and Read, M. S. (2017). Derivation of enhanced potentials for cerium brannerite and the calculation of lattice and intrinsic defect properties. *Nuclear Instruments and Methods in Physics Research Section B: Beam Interactions with Materials and Atoms,* **393**, 6367.

[16] Gale, J. D. (1997). GULP: A computer programme for the symmetry-adapted simulation of solids. Journal of the Chemical Society., Faraday TRANSACTIONS, 93, 629- 637.

[17] Minervini, L., Zacate, M. O., and Grimes, R. W. (1999). Defect cluster formation in M_2O_3-doped CeO_2. *Solid State Ionics,* **116**, 339-349.

[18] Catlow, C. R. A. (1997). Computer modelling in inorganic crystallography. Academic Press.

[19] Walker, J., and Catlow, C. R. A. (1981). Structural and dynamic properties of UO_2 at high temperatures. *Journal of Physics C: Solid State Physics*, **14**, 1979.

[20] Mott, N. and Littleton, M. (1989). Conduction in polar crystals: Electrolytic conduction in solid salts. *Journal of the Chemical Society, Faraday Transaction 2: Molecular and Chemical Physics*, **85**, 565-579.

[21] Read, M. S., Walker, S. R., and Jackson, R. A. (2014). Derivation of enhanced potentials for plutonium dioxide and the calculation of lattice and intrinsic defect properties. *Journal of Nuclear Materials*, **448**, 20-25.

[22] Lewis, G., and Catlow, C. (1986). Defect studies of doped and undoped barium titanate using computer simulation techniques. *Journal of Physics and Chemistry of Solids*, **47**, 89-97.

[23] Arima, T., Yamasaki, S, Inagaki. Y., and Idemitsu, K. (2005). Evaluation of thermal properties UO_2 and PuO_2 by equillibrium dynamics simulations from 300 to 2000 K. *Journal of Alloys and Compounds*, **400**, 43-93.

[24] March, N. H., (2013). Electron correlation in molecules and condensed phases. Springer Science & Business Media, New York, NY.

[25] Olsen, J. S., Gerward, L., Kanchana, V., and Vaitheeswaran, G. (2004). The bulk modulus of ThO_2 – an experimental and theoretical study, *Journal of Alloys and Compounds*, **381**, 3740.